Catena 216 (2022) 106401

Contents lists available at ScienceDirect

Catena

journal homepage: www.elsevier.com/locate/catena

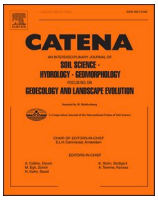

Characterising an abandoned phosphogypsum deposit by combining radiological, geophysical, geochemical, and statistical techniques

Marco D. Vásconez-Maza [a], María C. Bueso [b], Javier Mulas [c], Ángel Faz [d], Marcos A. Martínez-Segura [a,*]

[a] Department of Mining and Civil Engineering, Universidad Politécnica de Cartagena, Paseo Alfonso XIII, 52, 30203 Cartagena, Murcia, Spain
[b] Departamento de Matemática Aplicada y Estadística, Universidad Politécnica de Cartagena, Dr. Fleming s/n, 30202 Cartagena, Murcia, Spain
[c] Departamento de Ingeniería Térmica y Fluidos, Universidad Politécnica de Cartagena, Dr. Fleming s/n, 30202 Cartagena, Murcia, Spain
[d] Sustainable Use, Management and Reclamation of Soil and Water Research Group, ETSIA, Universidad Politécnica de Cartagena, Paseo Alfonso XIII, 48, 30203 Cartagena, Murcia, Spain

ARTICLE INFO

Keywords:
Characterisation
Electrical resistivity tomography
Phosphogypsum
Radiology
Uranium

ABSTRACT

Phosphoric fertiliser has enormously contributed to agriculture; however, it generates five tonnes of phosphogypsum per ton of phosphoric acid synthesised. Phosphogypsum houses heavy metals and long-lived radioactive elements that represents an environmental issue requiring remediation. This paper presents a methodology for characterising phosphogypsum deposits using geophysical, geochemical, and statistical tools. Gamma-ray probes determined the abnormal radioactive zones within the phosphogypsum deposits while electrical resistivity tomography provided the geometry and distribution of the phosphogypsum deposits. Chemical results confirmed the high presence of heavy metals in the waste determining chromium as the most concentrated metal. Radiological measures indicate that the effective ambient dose equivalent average in the study area surface is approximately 8.5 times higher than the average for Europe. While at 1.0 m depth, in the phosphogypsum layer, the ambient dose equivalent average surpasses approximately 27 times the European average. Statistical correlation analysis supports that the radiation increases due to the uranium presence. This methodology might reduce time and cost avoiding the use of expensive traditional methods, and it is exportable to any deposit.

1. Introduction

Phosphate compounds occur naturally on the earth, one of them is the apatite $Ca_5(PO_4)_3(OH,CL,F)$ that is commonly employed in fertiliser industry. Phosphoric based fertiliser have contributed enormously to farming industry. However, the production of fertiliser is linked to the generation of phosphogypsum as by-product. Phosphogypsum is a worldwide environmental issue, every year about 300 Mt are generated (Yang et al., 2016) which management differs in every country but only around 15% follow a recycling process (Silva et al., 2022) the rest in most of the cases remain in abandoned stacking areas.

Phosphogypsum stacking areas are usually placed near the coastlines exposed to weather and erosive agents being a potential hazard spot to human health and the environment (Lütke et al., 2020). These stacking areas can be found all around the world, from Imbituba in Brazil with about 4 Mt of phosphogypsum (Silva et al., 2022) to Huelva in the southeast of Spain which has 1200 ha fully covered by this by-product (Lieberman et al., 2020).

The physical and chemical features of the apatite vary depending on its geological origin (i.e. sedimentary or igneous). Phosphate rock is mined all around the world (e.g. Middle East, Morocco, India, China, USA, Brazil). Florida in the USA yields 19 Mt of phosphate rock every year (Liang et al., 2017); therefore, the amount of phosphogypsum increases aggravating the environmental issue every year.

The fertiliser industry employs the wet acid process that consists mainly of acidulating the rock with a strong acid. Sulphuric acid is the most common strong acid employed. Phosphate rock + sulphuric acid = phosphoric acid + phosphogypsum. Each ton of phosphoric acid involves the obtaining of five tonnes of phosphogypsum mainly composed of calcium sulphate ($CaSO_4{\cdot}2H_2O$) precipitated and trace elements which are potentially hazardous for both environment and human health.

* Corresponding author.
E-mail addresses: marco.vasconez@edu.upct.es (M.D. Vásconez-Maza), mcarmen.bueso@upct.es (M.C. Bueso), javier.mulas@upct.es (J. Mulas), angel.fazcano@upct.es (Á. Faz), marcos.martinez@upct.es (M.A. Martínez-Segura).

https://doi.org/10.1016/j.catena.2022.106401
Received 28 February 2022; Received in revised form 10 May 2022; Accepted 19 May 2022
Available online 28 May 2022

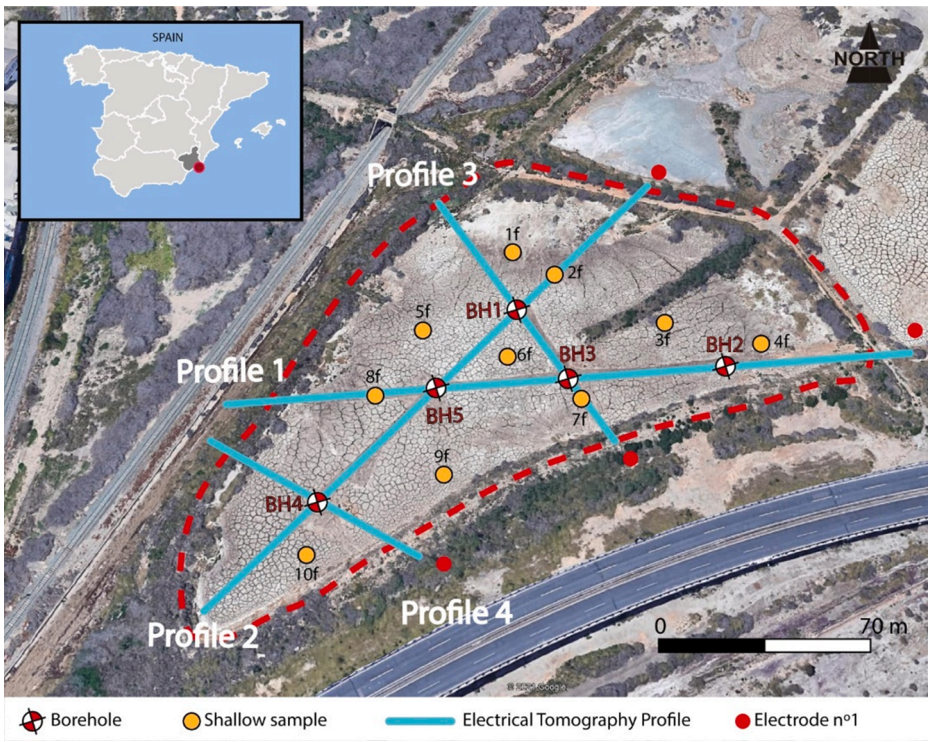

Fig. 1. Situation and aerial view of the study area. The red dashed line marks the studied phosphogypsum deposit, F1. Cian lines marks the electrical resistivity tomography (ERT) profiles, red dots mark the beginning of the ERT profile, red-white circles marks the boreholes, and orange dots mark the position of superficial sampling.

Natural radiation is present in phosphate rock that varies according to its geological genesis. Apatite with igneous origin presents lower radioactivity than sedimentary origin ranging between 40 and 5,000 Bq kg^{-1} (Chen, et al., 2003). The phosphate rock employed in this study came from Morocco; therefore, sedimentary origin. During the industrial process, phosphogypsum acquires heavy metals, radionuclides such as ^{238}U, ^{232}Th and its daughter nuclides, and ^{40}K depending on the origin of the phosphate rock (sedimentary) used as the input for the industrial (El Zrelli et al., 2019). Heavy metals could be available and could migrate to proximal urban/agricultural areas (Gabarrón et al., 2018). Therefore, natural radiation values increases within the phosphogypsum thus long exposure to it could affect human health (Rutherford et al., 1994).

Europe promotes legislation to provide safety standards for protection against ionising radiation. State members might guarantee the identification of activities or zones that utilise natural occurring radioactive materials. All necessary studies might be conducted to determine levels of radiation regarding protection of workers and public exposure. The council directive lists the industries involved with natural occurring radioactive materials. This study regards the waste generated by phosphate industry which is in the list of annex VI of the law (Official Journal of the European Union, 2013).

This paper presents the results of a characterisation not using conventional techniques rather a combination of geophysical, radiological, and statistical methods performed in a forsaken phosphogypsum area.

Consequently, this paper aims to: i) perform a physicochemical characterisation of an abandoned phosphogypsum pond using geochemical and geophysical techniques, ii) study the existing statistical relationships between data and iii) determine the radionuclide causing the rising of natural radiation values.

2. Materials and methods

2.1. Study area

The Campo de Cartagena in southeast of Spain. This area has a semiarid Mediterranean weather. The annual average weather values are: 17.6 °C of temperature, 313 mm of precipitation, and 2621 h of sun in a year (AEMET, 2020). The present study was carried out in an abandoned industrial area (El Hondón) near to Cartagena city that has an area of 113 ha approximately and a motorway divides the site into two parts. This area was an economical pole of Cartagena since the beginning of 20th century; many industrial activities have been performed there until 2001. Currently, several waste deposits of unknown volume and dimension cover the entire area; these deposits, mainly contain by-products of the synthesis of fertilisers from apatite through the wet acid process (pyrite and phosphogypsum). Among all deposits, the biggest phosphogypsum deposit was selected for this study, see Fig. 1.

Fig. 2 presents the geological map of the El Hondón area, east of Cartagena city. Near to the study area there is a small volcanic hill referred to as the "Cabezo de la Viuda" that is an excellent exponent of the alkaline basaltic volcanism stage that took place in the region at the end of the Pliocene and beginning of the Quaternary (Manteca, 2003). The Campo de Cartagena lies on a confined Quaternary aquifer counting with a big collection of "Ramblas" referred to as gravel-bed ephemeral stream where rainfall eventually runs (Martínez-Segura et al., 2021). The biggest Rambla in the Campo de Cartagena is the Rambla del Albujon and the nearest to the study area is the Rambla del Hondón (Alcolea et al., 2019).

2.2. Electrical resistivity tomography

Geophysics has several shallow techniques which before were prohibitive due to the high costs. Nowadays, near surface geophysics are

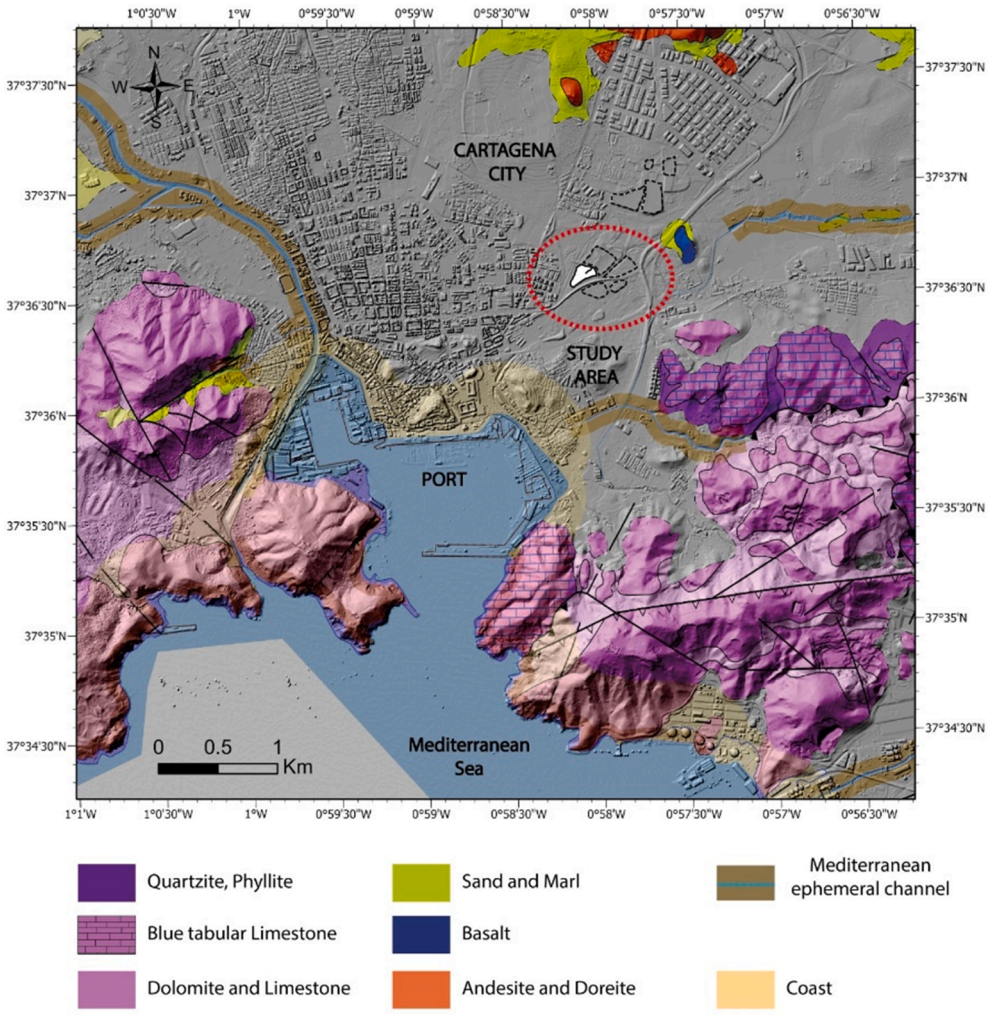

Fig. 2. Geological map of the study area ("El Hondón"). Coastline is marked with yellow colour. The read dashed line envelops the study area. Texture and colours of the legend mark the geological materials of the area. Gravel-bed ephemeral stream marked in cyan and yellow.

usually employed as a tool for performing environmental studies. One of these is the electrical resistivity tomography (ERT). This technique utilises electricity to generate electromagnetic fields by injecting controlled electrical currents and measuring the difference of potential externally. Researchers often choose ERT to perform environmental studies due to the speediness in data processing, the adaptability in the field and the affordability (Martín-Crespo et al., 2018; Martínez-Segura et al., 2020; Gabarrón et al., 2020).

Electrical resistivity tomography (ERT) uses electrical currents to assess the subsoil. A set of connected multi-electrodes injects currents and measures the difference of potential simultaneously. The interaction of these currents with the underground materials creates an electrical contrast allowing to compute 2D geoelectrical profiles (Everett, 2013). This study employed a Syscal R1 Switch 72 multi-core resistivimeter that is easy to transport and set in field, it is composed of four multi-core cables which hold eighteen electrodes (72 electrodes), a 12 V power supply, a laptop, and a high accuracy GPS. Wenner-Schlumberger array is often employed in ERT surveys because it has shown satisfactory results and it is a good compromise between horizontal and vertical resolution (Loke, 2015).

Four ERT profiles were deployed throughout the pond, referred to as F1. In this deposit, Profile 1 and Profile 2 employed 72 stainless electrodes, spacing each electrode in 3 m, reaching 213 m long. Profile 3 required 72 stainless electrodes too, but the span was 1.5 m, with 106.5 m long; and, Profile 4 only required 36 electrodes, separating by 2.5 m, reaching 87.5 m long, see Fig. 3.

Finally, field data are filtered with PROSYS II software, and the GPS coordinates of the electrodes are added. Next, the filtered data is inverted by using RES2DINV software, resulting in scaled georeferenced 2D geoelectrical profiles.

2.3. Geochemical characterisation

Geochemical characterisation was conducted on the surface and in the subsoil. Ten uniformly distributed composite samples (~1.0 kg) were collected on the surface of the pond about 0.3 m depth, see Fig. 1. Five boreholes were drilled in the pond using borehole core sampling machine with a diameter of perforation of 101 mm. These boreholes were conceived with ERT results to acquire samples where the electrical contrast presents significant changes. As a minimum, one borehole was situated on one geoelectrical ERT profile to guarantee a correlation among the data. This study used the local legal thresholds for metallic concentrations, referred to as NGR. All boreholes (1–5) have reached the natural terrain reaching 4.20 m, 5.40 m, 5.0 m, 6.0 m, and 5.0 m of depth, respectively.

Whole samples passed through a conditioning process before undergoing the laboratory procedure. Samples were dried for 72-hour at 35 °C, these samples were sieved to a 2 mm and ground with a Retsch RM 100 grinder. pH and electrical conductivity (EC) were measured in deionised water (1:2.5 w/v and 1:5 w/v). Metallic concentrations were

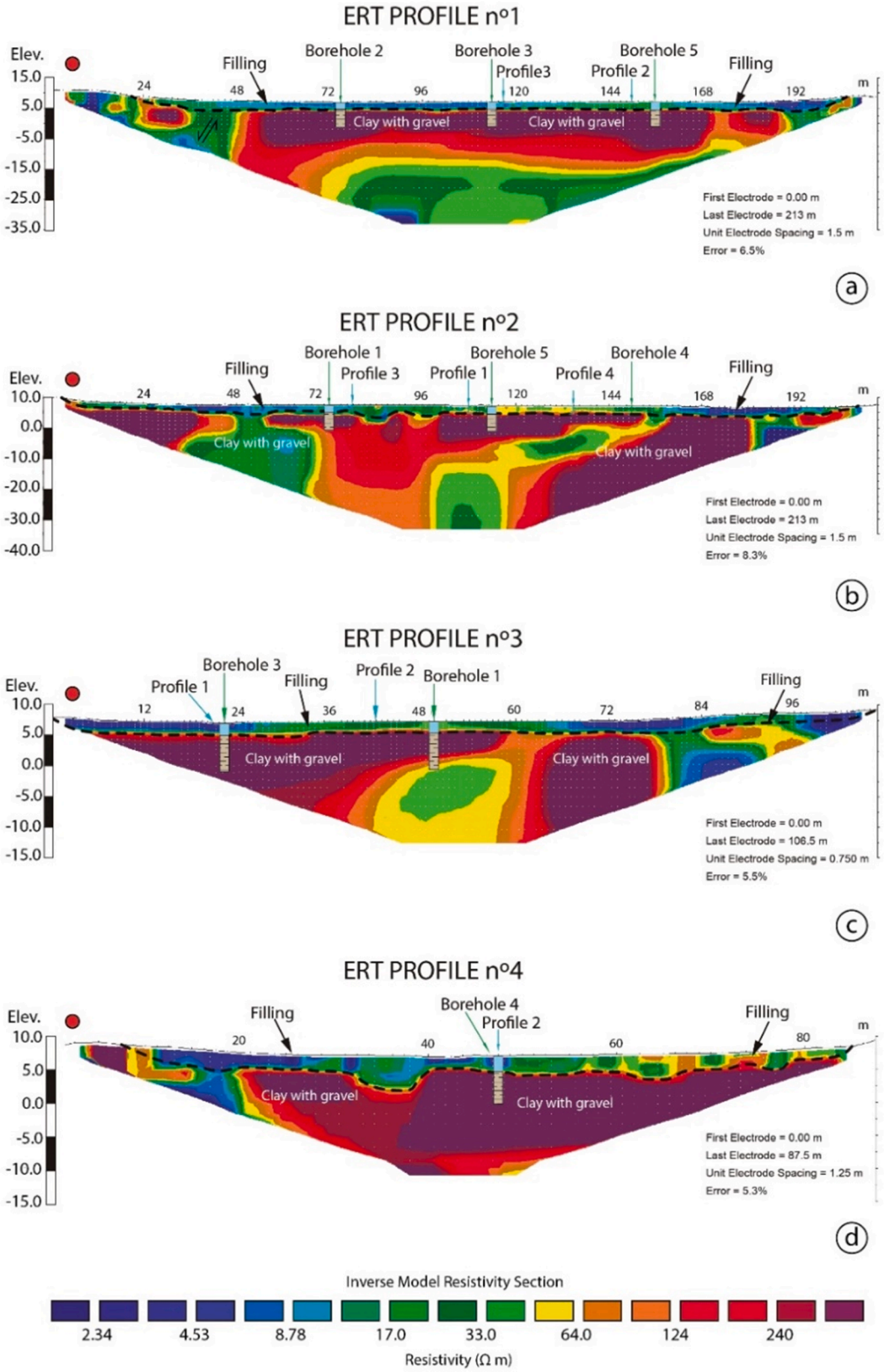

Fig. 3. Electrical resistivity tomography 2D sections and boreholes situation. a-d represents the ERT profiles obtained from deposit F1. Red dots mark the first electrode of the profile.

Table 1
Chemical results from borehole core samples for deposit F1.

Borehole	Depth m	Cd mg Kg^{-1}	Cr	Ni	Cu	As	Pb	Zn	Hg
BH1	0.0	22.7	313	72	49	33	7	153	6.9
	0.6	16.3	211	52	44	18	6	95	5.9
	1.5	10.1	616	64	59	29	28	233	5.9
	2.0	29.1	115	36	71	17	44	2109	0.3
	3.0	16.8	29	53	54	24	76	2106	0.3
	4.2	26.4	21	34	53	13	21	1608	0.2
BH2	0.0	16.7	347	57	137	28	8	158	9.5
	0.6	17.0	353	61	118	34	10	177	6.9
	1.5	9.3	849	82	119	28	12	234	9.2
	2.0	2.1	353	32	81	15	26	182	0.5
	2.4	1.9	22	29	72	10	11	38	0.3
	3.4	1.6	21	32	73	10	20	70	0.3
	4.2	1.1	26	37	70	14	46	151	0.4
	5.4	1.4	23	35	57	9	36	104	0.1
BH3	0.0	21.3	300	59	39	29	9	159	6.6
	0.8	20.5	540	71	40	35	6	266	5.5
	1.5	12.8	842	93	52	34	12	245	6.2
	2.2	4.8	24	77	21	10	37	112	0.2
	3.0	8.1	21	32	20	15	73	436	0.4
	4.2	5.0	29	33	26	22	106	602	0.4
	5.0	10.4	28	35	26	24	126	703	0.3
BH4	0.0	17.1	340	68	44	28	4	218	5.2
	1.0	13.4	470	53	32	30	6	150	4.5
	2.0	14.2	137	33	78	40	44	62	3.7
	3.3	2.1	21	54	19	12	23	77	0.4
	4.0	0.4	18	19	15	6	55	58	0.6
	5.0	0.4	23	28	30	5	31	65	0.7
	6.0	0.5	20	22	21	5	34	102	0.4
BH5	0.0	19.9	309	69	37	32	5	103	7.0
	0.6	16.5	471	85	39	30	4	143	9.8
	1.8	9.2	569	69	39	37	38	183	7.6
	2.4	2.2	54	27	33	51	17	46	0.3
	3.0	2.2	22	19	23	20	15	22	0.2
	4.0	13.2	21	36	26	15	44	64	0.4
	5.0	19.1	19	33	24	14	42	83	0.4
Mean		11.0	216.3	48.4	49.7	22.2	30.8	323.4	3.1
Min		0.4	17.6	18.6	15.2	4.7	3.7	22.3	0.1
Max		29.1	849.4	92.6	137.0	50.8	125.7	2109.0	9.8
SD		8.3	247.6	20.6	29.8	11.3	28.7	527.8	3.4
NGR		0.6	67	37	23	12	43	96.0	1.7

SD: Standard deviation. NGR: Local legal thresholds.

Table 2
Superficial radiological results at 1.0 m height. Bold values are the net dose calculated on the deposit measurement spot.

	Mean μSv h^{-1}	Variance μSv h^{-1}	SD μSv h^{-1}	Uncertainty (%)	Net dose μSv h^{-1}
01F1	0.977	0.018	0.136	13.9	**0.887**
02F1	0.930	0.002	0.044	4.7	**0.840**
03F1	1.250	0.001	0.034	2.7	**1.160**
04F1	1.026	$<10^{-3}$	0.019	1.9	**0.936**
05F1	1.475	$<10^{-3}$	0.022	1.5	**1.385**
06F1	0.775	$<10^{-3}$	0.008	1.1	**0.685**
07F1	0.548	$<10^{-3}$	0.011	1.5	**0.458**
08F1	0.647	$<10^{-3}$	0.014	1.6	**0.557**
09F1	1.012	0.002	0.044	4.3	**0.922**
10F1	0.895	0.016	0.103	11.4	**0.805**

* SD: Standard deviation.

extracted according to the US-EPA method 3051, (i.e., 0.5 g of sample in 10 ml of nitric acid (65%) and digested in a MARS 6 microwave) and the digested samples were read with an inductively coupled plasma-mass spectrometer (ICP-MS). The laboratory employed reference material (BAM-U110), blanks, reagents and duplicates during the analyses obtaining satisfactory recoveries ranging between 92% and 104%.

2.4. Radiological characterisation

The environmental equivalent dose rates were performed with several instruments, a portable Geiger Radex RD1503, was used to get approximative or coarse measures of the equivalent environmental dose rate in μSv h^{-1}, as a reference to identify the zones of interest, adjusting the alarm level to quickly locate areas with significative gamma radiation above the background.

The data for the shallow radiological study was acquired on the surface and at 1.0 m depth. The effective ambient dose equivalent H*(10) was measured on the surface. The measurements were done at 1.0 m height from the surface, placing the probe in an upright position using a light alloy tripod (aluminium) to avoid interferences, on which the multi-probe monitor was placed. For F1, there were ten points of measurement referred to as 1F1-10F1. Aiming to have an uncertainty of <10%, measurements lasted at least 10 min in each measurement point, measurements were automatically recorded every so often (5–10 s) obtaining a vast dataset per each point, see Table 2.

Ambient dose equivalent H*(10) was measured at 1.0 m depth within the boreholes previously drilled. The detector used was a RD4L radiation probe for measuring Gamma-X-ray radiation. The probe consists of a 25.0 × 25.0 mm scintillation detector of thallium-doped sodium iodide, and a photomultiplier. This is a high sensibility detector ranging from 5.0 nSv h^{-1} to 100.0 μSv h^{-1}measuring low activity gamma radiation. A MS6020-M multi-probe monitor has been used to read data from the probe (LAMSE, 2020). Calibration certificate number C216/4070

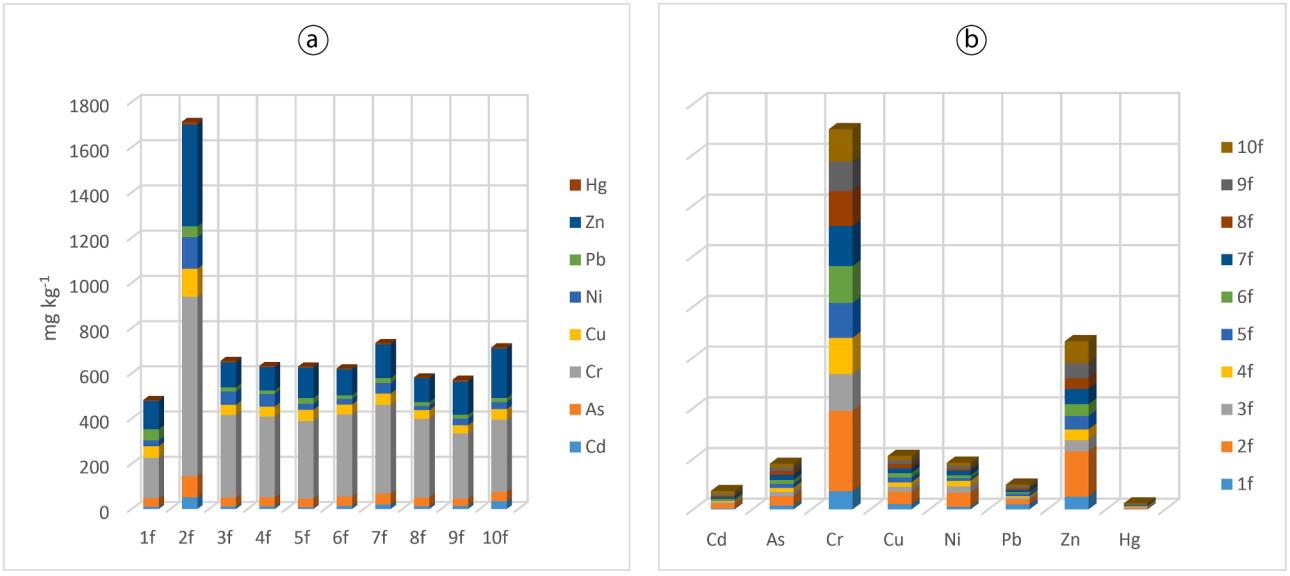

Fig. 4. Results from superficial chemical analysis. 1f-10f are the 10 samples gathered from the surface of the deposit. a) Cumulative metallic concentration per sample. b) Cumulative metallic concentration represented by metal analysed.

according the European standards (AENOR, 2019).

Geophysical equipment that uses natural gamma and spectral gamma probes is usually employed in the mining industry for identifying ore features. This study used previously drilled boreholes for the chemical analysis to perform the radiological characterisation. This procedure allowed assessing the phosphogypsum layer thickness identifying the place where the radiation activity varies.

Five boreholes were drilled after the ERT to carry out some chemical analysis. These boreholes were mapped out to be done on the ERT profiles or in the crossing point of two profiles facilitating the correlation of the data. Therefore, the measurements of specific activity, inside the boreholes, were carried out with QL40-GR (Natural Gamma Ray Probe) and QL40-SGR (Spectral Gamma Ray Probe) probes.

Gamma specific activity of natural radioisotopes ^{238}U, ^{232}Th and ^{40}K was gathered with probes, which measure various parameters and provide information about underground materials from the boreholes. These isotopes, along with their decay products, cause most of the gamma radiation in the phosphogypsum (Sahu et al., 2014). The equipment consists of two probes QL40-GR and QL40-SGR. Both probes are in a 6.0 kg cylindrical container (1.0 × 0.04 m). An electric controlled tripod allows inserting the device into the borehole controlling both speed and penetration depth. The device transmits the data to a computer using a connection cable, which records it with the corresponding software.

The QL40-GR probe consists of a 0.022 × 0.076 m highly luminescent scintillation crystal of thallium-doped sodium iodide and a photomultiplier, it performs the measurement of natural gamma radiation in the borehole. The QL40-SGR probe comprises a 0.025 × 0.102 m scintillation crystal of bismuth germanate (BGO) and a photomultiplier. The probe captures the gamma radiation spectra with 2,656 energy channels. It can discriminate contributions of ^{238}U, ^{232}Th and ^{40}K estimating the concentrations of the radioisotopes. Results are reported in API units which is the unit employed for natural gamma ray logs (Schlumberger Limited, 2020). The WellCAD and LoggerSuite software, by means of a mathematical algorithm, split the spectra. Obtaining results in different units: counts per second (cps), percentage (%), Becquerel per kilogram (Bq Kg^{-1}), and particles per million (ppm) (Terraplu Inc, 2020).

2.5. Statistical study

Statistical tools such as box-and-whisker plots and scatterplots were employed to figure out the global behaviour of the data. The statistical study was led with the R free statistical and graphical computing software (R Core Team, 2019). In the first stage, radiological data and resistivity data were analysed separately. Next, radiological data was narrowed down to fit into resistivity values for performing a correlation analysis. Spearman's rho coefficient was employed to identify monotonicity relationships among the variables based on the ranks of the data. Results were displayed in heatmaps.

Statistical tools are widely proven and employed to explore the global behaviour of the dataset and to find relationships and trends. In particular, correlation analysis have been employed for determining dependency between, mostly, ERT and radiological data.

3. Results and discussion

3.1. Electrical resistivity tomography

Boreholes core samples confirmed that the deposit was formed by accumulation thus, the variation expected is vertical but not horizontal. We have employed the Wenner-Schlumberger array because it provides both sufficient depth penetration and horizontal scope (Loke, 2015). Some authors (e.g. Martinez-Pagan et al., 2009; Mohammed and Abudeif, 2019) have employed this array in metallic waste deposits achieving satisfactory results. Effectively, on the top of the deposit lies the contaminated layer and at the bottom the natural terrain.

ERT Profiles 1–2 are the largest, they penetrated to a depth of about 45 m, while Profiles 3–4 reached until ≈25 m. The root mean square error (RMSE) indicates the quality of the inversion data; Rosales et al. (2012) point out that RMSE needs to be lower than 10% for considering the inversion as accurate. Then, our ERT profiles obtained has a RMSE lower than the 9% meeting the quality indicators. Fig. 3 presents the resulting ERT profiles of this study. A dashed line divides the top from the bottom layer. This line was drawn following the geometrical information provided from the borehole core samples, which are shown in the figure. The colour bar uses the rainbow as scale of colours, being the less resistive those colours closer to blue and those closer to red denoting higher resistivity.

The waste layer on the top of the deposit presents a relatively constant thickness ≈2.5 m. This waste layer appears in the four ERT profiles with similar characteristics showing resistivity values below 27 Ω m. Beneath the dashed line, the resistivity values rise over > 124 Ω m. This

bottom layer is composed of clay with gravels suggesting being the natural terrain. Some low resistivity values (<27 Ω m) appear in the bottom layer, notably, these low values mark an anomaly. Frid et al. (2017) state that ERT is a good technique to localise preferential leaching paths. We noticed a potential trait of leach in all ERT profiles (1–4) starting at ~ 36.0 m, ~48.0 m, ~80.0 m, and 10.0 m, respectively, see Fig. 3(a-d).

3.2. Properties and chemical composition of the deposits

Sulphuric acid (H_2SO_4) is widely employed in the fertiliser industry due to the calcium sulphate being much more insoluble (easier separation). During the wet acid process it occurs the following chemical reaction $Ca_{10}(PO_4)_6X_2 + 10H_2SO_4 + 20H_2O = 6H_3PO_4 + 10CaSO_4{\cdot}2H_2O + 2HX$ where X = Cl, F, OH (Lin et al., 2018). Consequently, in the precipitated $CaSO_4{\cdot}2H_2O$ remains a vast quantity of trace materials notably heavy metals accounting for the highly acidic behaviour with an average value of 3.9 and high levels of saline 10 ds m^{-1} of the deposit as Millán-Becerro et al. (2019) have found in their study.

The superficial chemical analysis yields the leading distinctive features regarding the metallic concentration which exceed the local legal thresholds (NGR) with the exception of lead. Fig. 4 provides a visual results summary of the 10 samples collected on the surface of the deposit. Notably, sample 2f is the most contaminated sample by heavy metals, see Fig. 4a and chromium is the metal that exhibits the highest concentration value with an average of 375 mg kg^{-1}, see Fig. 4b. We can highlight that lead presents values under its local legal threshold NGR (43 mg kg^{-1}) and the least concentrated metal is mercury but it surpasses by>3 times its NGR (1.7 mg kg^{-1}).

Pérez-López et al. (2016) allude that phosphogypsum is stacked in form of slurry, the subsequent dry process in a not fully waterproof deposit may lead to a leakage of phosphogypsum substances to the subsurface levels. We have observed that superficial chemical results suggest that a possible leach phenomenon is occurring from the top to the bottom of the deposit. On the surface lead shows an average value of 24 mg kg^{-1} which fits within the local legal thresholds (NGR). However, in all boreholes, lead presents a relative trend to increase in accordance with the depth, see Table 1.

As previously mentioned, borehole core samples have provided the geometry and the composition of the deposit. From the surface until about 2.0 m (waste layer) remains acidic and high in saline. In BH1, we have found evidence of the potential leaching phenomenon due to the higher values of Zn are located at the bottom of the borehole core sample between 2.0 and 4.0 m which accounts for the anomalies found during ERT survey. Similarly, occurs with lead in BH3, concentration of lead increases between 4.2 and 5.0 m of depth. Nonetheless, chromium presents a fixed trend in all boreholes high concentrations are on the top layer and it decrease in accordance with the depth, see table 1. The presence of the heavy metals in phosphogypsum could provide it an economic potential. El Zrelli et al. (2018) allude in their study to the possible economic exploitation of the phosphogypsum. Nevertheless, the elevated metallic concentration represents a potential hazard to the environment and human health due to these metals are available and could migrate to nearby urban nuclei (Gabarrón et al., 2018).

Also, waste containing heavy metals represents an environmental problem due to the potential contamination of nearby agricultural soils and the risk of the anomalous heavy metal concentration entering the food chain. Exposure to heavy metals could cause several illnesses. According to the Agency for Toxic Substances and Disease Registry (2011) cadmium exposure during pregnancy affects development, attacking the cardiovascular, gastrointestinal, neurological, renal, respiratory, and reproductive systems. Vásconez-Maza et al. (2019) summarise the health effects of the most common metals present in phosphogypsum.

Table 3
The ambient dose equivalent H*(10) at 1.0 m of depth within the boreholes with the probe RD4L.

Borehole	BH1 μSv h^{-1}	BH2	BH3	BH4	BH5	Total
Mean	3.602	3.152	2.863	3.347	2.890	**3.171**
SD	0.025	0.032	0.021	0.026	0.015	**0.022**

* SD: Standard deviation.

3.3. Radiological characterisation and statistical analysis

The presence of trace elements in phosphogypsum affects the subsoil as several authors have pointed out in their studies (Calin et al., 2015; El Zrelli et al., 2019; Jalali et al., 2019; Huang et al., 2020) Calculating the value of the effective ambient dose equivalent H*(10) it is mandatory to subtract the value of the radioactive background to the H*(10). The ambient dose equivalent H*(10) is 0.073 μSv h^{-1}, value determined in the MARNA project for the surroundings of the study area considering an average exposure value of 12 μR h^{-1} (CSN, 2005). Random sampling in the surroundings of the study area with the RD4L radiation probe gave 0.09–0.11 μSv h^{-1}. These results are consistent with 0.11 μSv h^{-1}, which is the monthly average measure for Murcia region provided by the national regulatory authority (CSN, 2019). Thus, for this study, we consider 0.09 μSv h^{-1}as the background radiation.

Furthermore, Table 2 summarises the results of effective ambient dose equivalent H*(10) measured in the field at 1.0 m height. The global net mean of effective ambient dose equivalent H*(10) is 0.9089 μSv h^{-1} at 1.0 m. According to the Official Journal of the European Union (2013) member states shall set the limit on the effective dose for public exposure at 1.0 mSv in a year. Transforming our results in millisieverts per year, we have obtained 7.961 mSv/y at 1.0 m, as expected for phosphogypsum deposits.

Measurements performed inside the boreholes we have; on the one hand, the dose rate was measured by inserting the RD4L equipment. This equipment was inserted 1.0 m as maximum depth due to the specific activity measured with QL40 probe started at that depth. Table 3 presents the result of those measurements; the standard deviation is acceptable in all cases resulting in an average dose equivalent H*(10) of 27.7676 mSv/y. As expected, the dose surpasses the annual limit for public exposure both on the surface as well as inside of boreholes due to the composition of the phosphogypsum (Ministerio de Industria y Energía, 1999).

On the other hand, the underground radioactivity measurements performed with QL40 probe gives results in API units which can be transformed into cps, Bq kg^{-1}, ppm and %, as aforementioned. Scatterplots of the results visually presented a significant association among the data (Fig. 5a). Therefore, a correlation analysis was carried out to distinguish which one of the radionuclides is causing the rising of the radiation, results are displayed in heatmaps (Fig. 5b). The Spearman's correlation coefficient showed a strong and positive significant correlation with the Uranium in all boreholes, see Fig. 5c. For the borehole BH1 refer to Fig. 5 (a,b).

The national regulatory authority (CSN, 2011) alludes that the radioactivity of the phosphogypsum from Huelva (Spain Southwest) is caused mainly by the uranium. Since the ancient fertiliser plant utilised the same raw phosphoric rock as Huelva, we expect similar results. This radiological activity is coherent with the reality, it rises in the point where the phosphogypsum layer is located and the activity values decrease where the layer ends, and the natural terrain layer starts. The profiles of specific activity obtained with QL40 probes are compared with the lithological reports from the boreholes, and the correlation between them is reliable. Depth of the materials interfaces and the decrease in activity detected are linked. In deposit F1 the thickness of the phosphogypsum layer is constant until the depth of 2.0 m. then, it reaches deeper until around 2.9 m. In some cases, the concentration of

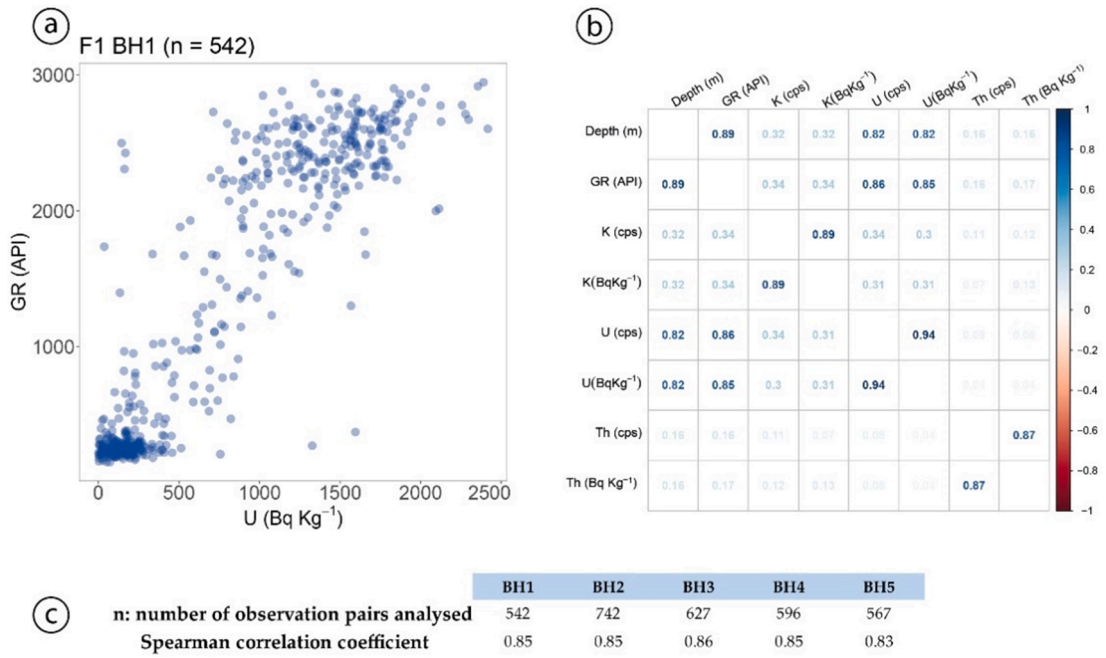

c

	BH1	BH2	BH3	BH4	BH5
n: number of observation pairs analysed	542	742	627	596	567
Spearman correlation coefficient	0.85	0.85	0.86	0.85	0.83

Fig. 5. a) Scatterplot of variables. b) Spearman correlation heatmap for F1 and BH1. c) Values of the Spearman correlation coefficient computed between API with Uranium (U).

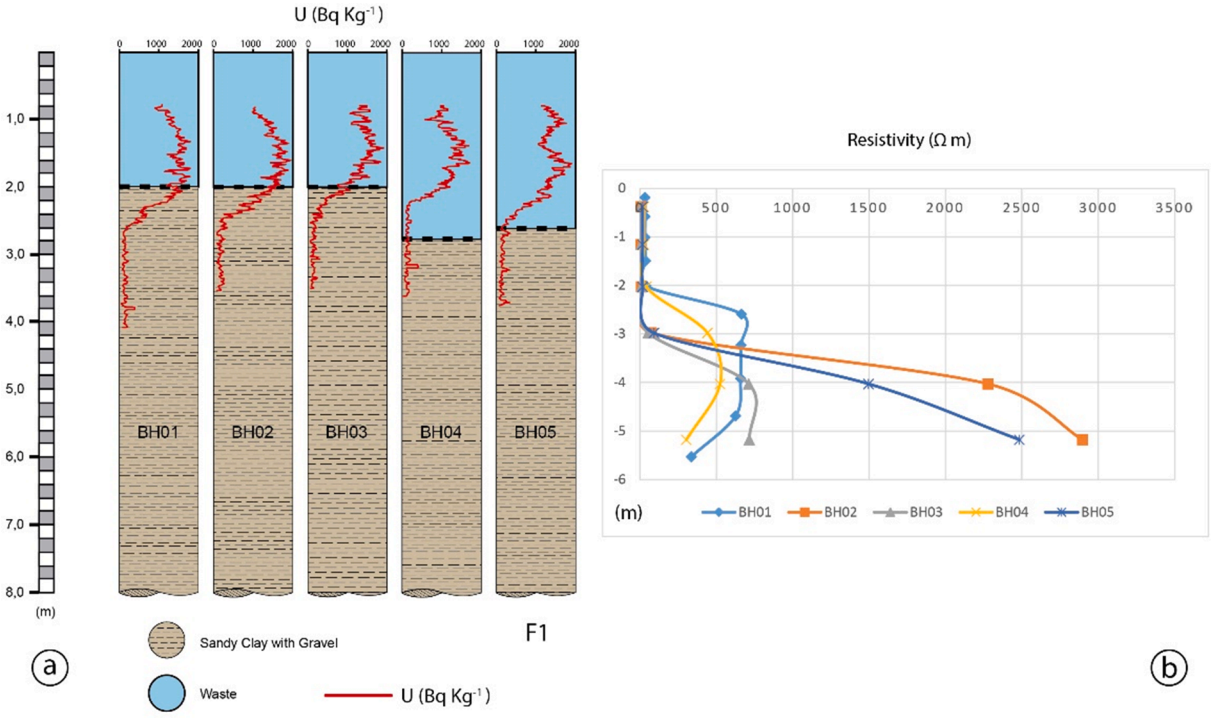

Fig. 6. a) Lithology obtained from boreholes compared with 2D profiles of specific activity for the deposit F1. b) Curves of electrical resistivity tomography from deposit F1.

^{238}U reaches below the waste layer; a possible explanation is that some material has leached dragging ^{238}U into subsoil areas, although in any case it is within the 0.5 m gamma influence zone, see Fig. 6a. Curves of electrical resistivity tomography from deposit F1 (Fig. 6b) presents values low resistivity values (<27.0 Ω m) in the first meters of the deposit which corresponds to the waste layer. Resistivity values increase since 2–3 m of depth corresponding with the natural terrain.

3.3.1. New findings: Statistical correlation between radioactivity and ERT.

Pursuing the correlational analysis, we find out that ERT values have significant correlations with the radioactivity. The ERT data limit the radiological data; therefore, we narrowed down the data, and we carried out the analysis with just the data located in the outlying of ERT.

Deposit F1 has a total of 3,074 observation pairs to discriminate the radionuclide causing the specific activity (Spearman's coefficient) while only 105 observation pairs for correlating API with ERT, opening a new

Table 4
Values of the Spearman correlation coefficient computed between radiation (API) with electrical resistivity (Re) and radiation (API) with Uranium (U).

		Spearman correlation coefficient	
Borehole	**n**	**Re**	**U**
BH1	16	**−0.72**	0.76
BH2	12	**−0.91**	0.49
BH3	12	**−0.91**	0.77
BH4	45	**−0.44**	0.85
BH5	20	**−0.28**	0.85

n: number of observation pairs analysed.

line of investigation but further and detailed studies must be conducted to corroborate this association.

Even though the number of observations has dropped drastically when the resistivity variable is added to the analysis, the correlation coefficients continue being significant in most of the cases. Variables did not present a clear linear relationship; therefore, it was employed Spearman's coefficient that detected the monotonicity of relationships. We use as a criterion the correlation between radioactivity (API) and electrical resistivity (Re) due to the ERT is not able to distinguish among the specific activity of each isotope. Table 4 presents results from the analysis, bolded column marks the results of the correlation between Re and API.

4. Conclusions

The characterisation of the phosphogypsum deposit was successfully carried out using geophysical, geochemical, and statistical techniques. Even though all the analysed metals but lead exceed by far the local legal thresholds (NGR) on the surface of the deposit, the chemical analysis allowed identifying the most concentrated metals within the deposit. Evaluating the borehole core samples and the superficial samples, we can conclude that chromium is the most concentrated metal with 375 mg kg^{-1} on the surface and the concentration decreases in accordance with the depth reaching values below 30 mg kg^{-1}. The ERT provided the geometry of the deposits, identifying two layers being the top layer the most contaminated that is linked to low resistivity values (<27 Ω m) and the bottom of the natural terrain featured by higher resistivity values > 124 Ω m. Boreholes validated the ERT results, and the different gamma ray probes provided the radiological values of the study area. Radiological measures indicate that the average radiation dose surpasses the national average dose of radiation. Consequently, we can consider that geophysical techniques could be a useful tool for the radiological characterisation of phosphogypsum deposits.

By performing the correlational analysis, we were able to confirm the initial hypothesis, identifying the ^{238}U as the principal radionuclide causing the specific activity within the phosphogypsum. Also, correlating radiological data with electrical resistivity values we found a possible association opening a new research line for further studies. Therefore, it can be concluded that this study set an efficient methodology to characterise phosphogypsum deposit and this methodology can be exported to any other deposit.

Declaration of Competing Interest

The authors declare that they have no known competing financial interests or personal relationships that could have appeared to influence the work reported in this paper.

References

AEMET, 'Valores climatológicos normales: San Javier Aeropuerto', 2020. http://www.aemet.es/es/serviciosclimaticos/datosclimatologicos/valoresclimatologicos?l=7031&k=mur (accessed Feb. 20, 2020).

AENOR, Radiation protection instrumentation - Ambient and/or directional dose equivalent (rate) meters and/or monitors for beta, X and gamma radiation - Part 2: High range beta and photon dose and dose rate portable instruments for emergency radiation protection. Spain, 2019.

Agency for Toxic Substances and Disease Registry, 'ATSDR - Substance Listing Page', 2011. https://www.atsdr.cdc.gov/substances/indexAZ.asp (accessed May 31, 2019).

Alcolea, A., Contreras, S., Hunink, J.E., García-Aróstegui, J.L., Jiménez-Martínez, J., 2019. Hydrogeological modelling for the watershed management of the Mar Menor coastal lagoon (Spain). Sci. Total Environ. 663, 901–914. https://doi.org/10.1016/j.scitotenv.2019.01.375.

Calin, M.R., Radulescu, I., Calin, M.A., 2015. Measurement and evaluation of natural radioactivity in phosphogypsum in industrial areas from Romania. J. Radioanal. Nucl. Chem. 304 (3), 1303–1312. https://doi.org/10.1007/s10967-015-3970-3.

Chen, Q. et al., 2022. Effluent and dose control from European Union NORM industries: assessment of current situation and proposal for a harmonised Community approach : volume 1, main report. Luxembourg: Publications Office, 2003. Accessed: May 02, 2022. [Online]. Available: http://bookshop.europa.eu/uri?target=EUB:NOTICE:KO14003001:EN:HTML.

CSN, 'Proyecto Marna. Mapa de radiación gamma natural', Madrid, 2005.

CSN, 'Valores ambientales REA', Sep. 01, 2019. https://www.csn.es/valores-ambientales-rea (accessed May 28, 2020).

CSN, 2011. 'Estudio y evaluación del impacto radiológico producido por las actividades de diversas industrias no nucleares del sur de España. Industrias de ácido fosfórico', Madrid, 2011.

El Zrelli, R., Rabaoui, L., Daghbouj, N., Abda, H., Castet, S., Josse, C., van Beek, P., Souhaut, M., Michel, S., Bejaoui, N., Courjault-Radé, P., 2018. Characterization of phosphate rock and phosphogypsum from Gabes phosphate fertilizer factories (SE Tunisia): high mining potential and implications for environmental protection. Environ. Sci. Pollut. Res. 25 (15), 14690–14702. https://doi.org/10.1007/s11356-018-1648-4.

El Zrelli, R., Rabaoui, L., van Beek, P., Castet, S., Souhaut, M., Grégoire, M., Courjault-Radé, P., 2019. Natural radioactivity and radiation hazard assessment of industrial wastes from the coastal phosphate treatment plants of Gabes (Tunisia, Southern Mediterranean Sea). Mar. Pollut. Bull. 146, 454–461. https://doi.org/10.1016/j.marpolbul.2019.06.075.

El Zrelli, R., Rabaoui, L., Abda, H., Daghbouj, N., Pérez-López, R., Castet, S., Aigouy, T., Bejaoui, N., Courjault-Radé, P., 2019. Characterization of the role of phosphogypsum foam in the transport of metals and radionuclides in the Southern Mediterranean Sea. J. Hazard. Mater. 363, 258–267. https://doi.org/10.1016/j.jhazmat.2018.09.083.

Everett, M.E., 2013. Near-Surface Applied Geophysics. Cambridge University Press.

Frid, V., Sharabi, I., Frid, M., Averbakh, A., 2017. Leachate detection via statistical analysis of electrical resistivity and induced polarization data at a waste disposal site (Northern Israel). Environ. Earth Sci. 76 (6), 233. https://doi.org/10.1007/s12665-017-6554-4.

Gabarrón, M., Faz, A., Acosta, J.A., 2018. Use of multivariable and redundancy analysis to assess the behavior of metals and arsenic in urban soil and road dust affected by metallic mining as a base for risk assessment. J. Environ. Manage. 206, 192–201. https://doi.org/10.1016/j.jenvman.2017.10.034.

Gabarrón, M., Faz, A., Martínez-Martínez, S., Acosta, J.A., 2018. Change in metals and arsenic distribution in soil and their bioavailability beside old tailing ponds. J. Environ. Manage. 212, 292–300. https://doi.org/10.1016/j.jenvman.2018.02.010.

Gabarrón, M., Martínez-Pagán, P., Martínez-Segura, M., Bueso, M., Martínez-Martínez, S., Faz, Á., Acosta, J., 2020. Electrical resistivity tomography as a support tool for physicochemical properties assessment of near-surface waste materials in a mining tailing pond (El Gorguel, SE Spain). Minerals 10 (6), 559. https://doi.org/10.3390/min10060559.

Y. Huang et al., Phosphogypsum as a component of calcium sulfoaluminate cement: hazardous elements immobilization, radioactivity and performances, J. Clean. Product. 248(2020), doi: 10.1016/j.jclepro.2019.119287.

Jalali, J., Gaudin, P., Capiaux, H., Ammar, E., Lebeau, T., 2019. Fate and transport of metal trace elements from phosphogypsum piles in Tunisia and their impact on soil bacteria and wild plants. Ecotoxicol. Environ. Saf. 174, 12–25. https://doi.org/10.1016/j.ecoenv.2019.02.051.

LAMSE, 'Instruments for radiation detection and measurement', 2020. http://www.lamse.es/index-eng (accessed May 23, 2020).

Liang, H., Zhang, P., Jin, Z., DePaoli, D., 2017. Rare-earth leaching from Florida phosphate rock in wet-process phosphoric acid production. Miner. Metall. Process. 34 (3), 146–153. https://doi.org/10.19150/mmp.7615.

Lieberman, R.N., Izquierdo, M., Córdoba, P., Moreno Palmerola, N., Querol, X., Sánchez de la Campa, A.M., Font, O., Cohen, H., Knop, Y., Torres-Sánchez, R., Sánchez-Rodas, D., Muñoz-Quiros, C., de la Rosa, J.D., 2020. The geochemical evolution of brines from phosphogypsum deposits in Huelva (SW Spain) and its environmental implications. Sci. Total Environ. 700, 134444. https://doi.org/10.1016/j.scitotenv.2019.134444.

Schlumberger Limited, 'API unit - Schlumberger Oilfield Glossary', 2020. https://www.glossary.oilfield.slb.com/en/Terms/a/api_unit.aspx (accessed May 24, 2020).

Lin, J., Sun, W., Desmarais, J., Chen, N., Feng, R., Zhang, P., Li, D., Lieu, A., Tse, J.S., Pan, Y., 2018. Uptake and speciation of uranium in synthetic gypsum (CaSO 4 •2H 2 O): Applications to radioactive mine tailings. J. Environ. Radioactivity 181, 8–17. https://doi.org/10.1016/j.jenvrad.2017.10.010.

M.H. Loke, Tutorial:2-D and 3-D Electrical Imaging Surveys, Tutorial, 2015. http://citeseerx.ist.psu.edu/viewdoc/download?doi=10.1.1.454.4831&rep=rep1&type=pdf (accessed Mar. 05, 2019).

Lütke, S.F., Oliveira, M.L.S., Silva, L.F.O., Cadaval, T.R.S., Dotto, G.L., 2020. Nanominerals assemblages and hazardous elements assessment in phosphogypsum from an abandoned phosphate fertilizer industry. Chemosphere 256, 127138. https://doi.org/10.1016/j.chemosphere.2020.127138.

J. I. Manteca, 'DESARROLLO URBANÍSTICO VERSUS PATRIMONIO GEOLÓGICO', in *2003*, Utrillas, p. 9. [Online]. Available: blob:https://web.whatsapp.com/193e27a8-bddc-4c48-a904-96f411b92641.

Martín-Crespo, T., Gómez-Ortiz, D., Martín-Velázquez, S., Martínez-Pagán, P., De Ignacio, C., Lillo, J., Faz, Á., 2018. Geoenvironmental characterization of unstable abandoned mine tailings combining geophysical and geochemical methods (Cartagena-La Union district, Spain). Eng. Geol. 232, 135–146.

Martinez-Pagan, P., Cano, A.F., Aracil, E., Arocena, J.M., 2009. Electrical resistivity imaging revealed the spatial properties of mine tailing ponds in the sierra Minera of Southeast Spain. J. Environ. Eng. Geophys. 14 (2), 63–76. https://doi.org/10.2113/JEEG14.2.63.

Martínez-Segura, M.A., Vásconez-Maza, M.D., García-Nieto, M.C., 2020. Volumetric characterisation of waste deposits generated during the production of fertiliser derived from phosphoric rock by using LiDAR and electrical resistivity tomography. Sci. Total Environ. 716, 137076. https://doi.org/10.1016/j.scitotenv.2020.137076.

Martínez-Segura, M.A., Conesa-García, C., Pérez-Cutillas, P., Martínez-Pagán, P., Vásconez-Maza, M.D., 2021. Identifying changes in sediment texture along an ephemeral gravel-bed stream using electrical resistivity tomography 2D and 3D. Appl. Sci. 11 (7), 3030. https://doi.org/10.3390/app11073030.

Millán-Becerro, R., Pérez-López, R., Macías, F., Cánovas, C.R., Papaslioti, E.-M., Dolores Basallote, M., 2019. Assessment of metals mobility during the alkaline treatment of highly acid phosphogypsum leachates. Sci. Total Environ. 660, 395–405.

Ministerio de Industria y Energía, Real Decreto 1836/1999, de 3 de diciembre, por el que se aprueba el Reglamento sobre instalaciones nucleares y radiactivas. 1999, pp. 1–42.

Mohammed, M.A., Abudeif, A.M., 2019. Geoelectrical characterization of the Al-Kawamil New Settlement, Sohag, Egypt. J. Environ. Eng. Geophys. 24 (2), 327–332. https://doi.org/10.2113/JEEG24.2.327.

Official Journal of the European Union, *COUNCIL DIRECTIVE 2013/59/EURATOM of 5 December 2013*. Publication Office of the European Union, 2013.

Pérez-López, R., Macías, F., Cánovas, C.R., Sarmiento, A.M., Pérez-Moreno, S.M., 2016. Pollutant flows from a phosphogypsum disposal area to an estuarine environment: an insight from geochemical signatures. Sci. Total Environ. 553, 42–51. https://doi.org/10.1016/j.scitotenv.2016.02.070.

R Core Team, 'R: A language and environment for statistical computing. R Foundation for Statistical Computing', 2019. https://www.r-project.org/ (accessed Oct. 30, 2019).

Rosales, R.M., Martínez-Pagan, P., Faz, A., Moreno-Cornejo, J., 2012. Environmental monitoring using electrical resistivity tomography (ERT) in the subsoil of three former petrol stations in SE of Spain. Water Air Soil Pollut. 223 (7), 3757–3773. https://doi.org/10.1007/s11270-012-1146-0.

Rutherford, P.M., Dudas, M.J., Samek, R.A., 1994. Environmental impacts of phosphogypsum. Sci. Total Environ. 149 (1–2), 1–38. https://doi.org/10.1016/0048-9697(94)90002-7.

Sahu, S.K., Ajmal, P.Y., Bhangare, R.C., Tiwari, M., Pandit, G.G., 2014. Natural radioactivity assessment of a phosphate fertilizer plant area. J. Radiat. Res. Appl. Sci. 7 (1), 123–128. https://doi.org/10.1016/j.jrras.2014.01.001.

Silva, L.F.O., Oliveira, M.L.S., Crissien, T.J., Santosh, M., Bolivar, J., Shao, L., Dotto, G.L., Gasparotto, J., Schindler, M., 2022. A review on the environmental impact of phosphogypsum and potential health impacts through the release of nanoparticles. Chemosphere 286, 131513. https://doi.org/10.1016/j.chemosphere.2021.131513.

Terraplu Inc, 2020. You searched for wellcad - Terraplus: Geophysical Equipment Supplier, 2020. https://terraplus.ca/?s=wellcad (accessed May 23, 2020).

Vásconez-Maza, M.D., Martínez-Segura, M.A., Bueso, M.C., Faz, Á., García-Nieto, M.C., Gabarrón, M., Acosta, J.A., 2019. Predicting spatial distribution of heavy metals in an abandoned phosphogypsum pond combining geochemistry, electrical resistivity tomography and statistical methods. J. Hazardous Mater. 374, 392–400. https://doi.org/10.1016/j.jhazmat.2019.04.045.

Yang, L., Zhang, Y., Yan, Y., 2016. Utilization of original phosphogypsum as raw material for the preparation of self-leveling mortar. J. Cleaner Prod. 127, 204–213. https://doi.org/10.1016/j.jclepro.2016.04.054.